Surface Jumping: Franck−Condon Factors and Condon Points in Phase Space

S. Kallush,[†] Bilha Segev,*[,†] A. V. Sergeev,[†] and E. J. Heller*[,‡]

Department of Chemistry, Ben-Gurion University of the Negev, POB 653, Beer-Sheva 84105, Israel, and Departments of Chemistry and Physics, Harvard University, Cambridge, Massachusetts 02138

Received: November 29, 2001; In Final Form: March 27, 2002

We generalize the concept of Tully−Preston surface hopping to include larger *jumps* in the case that the surfaces do not cross. Instead of identifying a complex hopping point, we specify a jump between two locales in phase space. This concept is used here to find propensity rules for the accepting vibrational mode(s) in a radiationless vibronic relaxation transition. A model inspired by the $S_2 \rightarrow S_0$ vibronic relaxation transition of the benzene molecule in which 30 modes of vibration compete for the electronic energy is studied within this approach. For this model, we show that almost all of the energy must go to a single C−H local stretching. The initial conditions for vibrations of this mode are a coordinate jump of the hydrogen atom toward the ring. All of the other modes undergo an almost vertical transition, in which the energy that they take is determined by their equilibrium displacement between the two surfaces. We observe that for a large energy gap the masses and frequencies become the defining parameters for choosing the accepting mode. Anharmonicities are very important when a competition between degenerate modes occurs. These conclusions are demonstrated by the specific model considered here but apply in general to any weak internal conversion process.

1. Introduction

Molecular electronic transitions may be radiative or nonradiative. In either case, the process may be Franck−Condon enhanced or suppressed. The enhanced processes correspond to a crossing of Born−Oppenheimer potential energy surfaces in the classically accessible region, whereas Franck−Condon suppressed events have no such crossing. Examples include radiative processes in the wings of absorption or emission band envelopes and radiationless events for nested potential energy surfaces.

We focus here on intuition and procedures for realistic polyatomic processes. For the case of surface crossing, or avoided crossing, the Tully−Preston surface hopping[1] picture has been of considerable value, permitting both intuition and simple procedures for calculating rates of electronic conversion. Some extensions of this approach and insight can be found in refs 2 and 3.

When the surfaces cross, trajectories can hop smoothly with little or no change in position or momentum at the time of the hop. But often surfaces do not cross. What then? Of course, the rate for such cases is generally lower because of the implied suppression of Franck−Condon (FC) factors. However, these suppressed events may be "the only game in town" or may be significant channels competing with others.[4] Analytical continuation is sometimes used in these cases to recognize a complex jumping point in coordinate space,[5,6] and quasiclassical models are also useful,[7] but we want a more direct procedure that is applicable to many degrees of freedom. The approach we use is surface jumping.[8]

Our paradigm in this paper is a radiationless transition between nested surface potentials as shown in Figure 1b. This

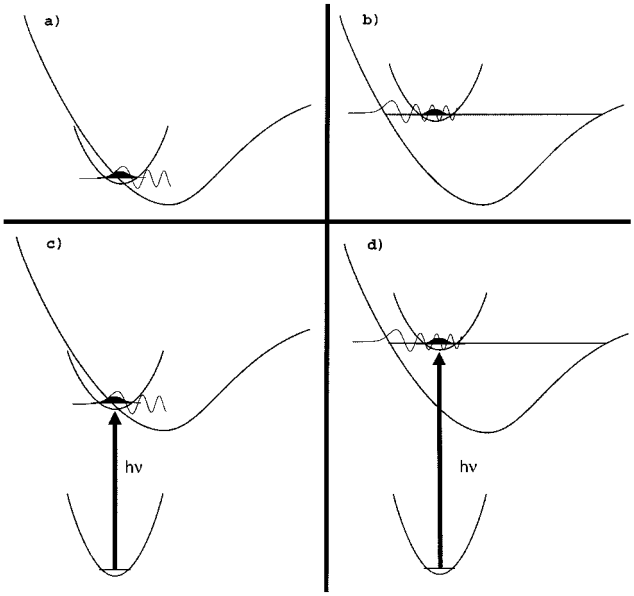

Figure 1. Two kinds of transitions: vertical and nonvertical. Panel a shows radiationless vertical transition between crossing surfaces. The transition takes place by continuous changes of the coordinates and via the point of crossing between the surfaces. Panel b shows radiationless nonvertical transition for nested surfaces—surface jumping. The transfer of the energy must occur by a sudden change of position or momentum. The direction of the jump is not obvious a priori. Our purpose is to predict this direction. Panel c shows radiative vertical transition equivalent to the radiationless case in panel a: most of the energy goes to the emitted photon. The transition takes place by continuous changes of the coordinates and via the point of crossing between the dressed initial surface and the final accepting energy surface. Panel d shows radiative nonvertical transition equivalent to the radiationless case in panel b: such transitions occur in the blue wing of an absorption band, where some of the energy of the absorbed photon is transferred into vibrational energy via surface jumping.

* To whom correspondence should be addressed. E-mail addresses: bsegev@bgumail.bgu.ac.il or heller@physics.harvard.edu.
[†] Ben-Gurion University of the Negev.
[‡] Harvard University.

10.1021/jp014336m CCC: $22.00
Published on Web 06/04/2002

situation can also arise radiatively, if we consider, say, the upper surface to be raised past the absorption maximum by the photon energy $h\nu$ as in Figure 1d. We have in mind a many-coordinate example.

Perhaps it is not obvious that any useful classical picture can emerge for this noncrossing situation, because the situation that we describe is classically forbidden. However, other classically forbidden processes have very useful classical descriptions, such as barrier tunneling, which involves trajectories in imaginary time or on the inverted potential energy surface.

Recently, some of us have outlined a procedure to recognize the jumping points in phase space in the noncrossing regime.[8,9] We demonstrated the method by applying it to a two-dimensional harmonic oscillator, a model in which one can find the jumping point analytically.[8] The results were encouraging. Identification of the jumping points was shown to allow for an easy derivation of propensity rules for the distribution of the electronic energy between competing vibrational modes. The treatment was limited in two ways: first by the assumption of harmonic potentials and second by the assumption of an allowed transition with no derivative coupling between the states. Here, we generalize the treatment to transitions between any two multidimensional, nonharmonic potentials and establish the numerical tools that are needed for the recognition of the jumping points in the general case. We also generalize the treatment so that it applies to internal conversion, that is, electronically forbidden transitions induced by derivative couplings, and study what is then the contribution of the promoting mode.

Questions that we address in this paper are as follows: Where will the jump between the two surfaces take place? What is the best system of coordinates to describe the process? What is the sensitivity of these predictions to the value of various parameters? The importance of the absolute value of the frequency and the reduced mass of a mode in the determination of its propensity as an accepting mode was previously discussed[10,11] with implications for the isotope effect for nonradiative decay.[11] Here, we supplement these early studies by considering the transition in phase space.

As an example, we apply our approach to a model inspired by a complex physical system, the 30 modes problem of the $S_2 \rightarrow S_0$ transition of the benzene molecule. As detailed below, the model imitates some properties of the benzene molecule yet differs from it in some other features. While it is not a complete description of the benzene molecule, much can be learned from it nevertheless. Even for this simplified model of the $S_2 \rightarrow S_0$ transition, it is not trivial to determine which modes or combination of the 30 vibrational modes of our system would be first excited during the quantum jump. With the new surface-jumping approach, we are able to do so with relative ease.

The outline of the paper is as follows: Surface jumping is defined and analyzed in section II. In section III, we apply the method to a model of an $S_2 \rightarrow S_0$ transition inspired by the benzene molecule and study the sensitivity of the results to different conjectures regarding the surface potentials. Section IV concludes and summarizes.

2. Franck−Condon Factors in Phase Space

2.1. Quantum-Mechanical Treatment in Coordinate Space. The probability for an allowed transition from the vibronic state i to a vibronic manifold j, where i, j refer to electronic states, is given by

$$P^{i\rightarrow j} = |\mu_{\mathrm{elec}}|^2 \sum_{\{n_k'\}} \prod_k |\langle \chi^j_{n_k'} | \chi^i_{n_k} \rangle|^2 \quad (1)$$

Here, $\mu_{\mathrm{elec}} = \int \psi_j^* \hat{\mu}_{\mathrm{elec}} \psi_i \, \mathrm{d}\vec{r}$ is the dipole transition moment between the electronic states ψ_i and ψ_j and $\hat{\mu}_{elec}$ is the dipole moment operator. The integration $\mathrm{d}\vec{r}$ is over all of the electronic coordinates $\vec{r}$. The nuclear wave function for the mode q_k in the electronic state i for vibrationally excited state n_k is $\chi^i_{n_k}$, and separability is assumed. Separability is not necessary for our approach, and we do not use it below for the final state, but here, we use it for simplicity. The term $\prod_k |\langle \chi^j_{n'_k} | \chi^i_{n_k} \rangle|^2$ in this expression is the FC factor squared between two vibronic states. The summation, $\sum_{\{n_k'\}}$, is over a manifold of vibronic states, of which the energy is equal to the energy of the initial state i. Note that an excited initial state, as considered here, has a finite energy width allowing for many final states with slightly different energies. For internal conversion, an electronically forbidden transition, $\mu_{\mathrm{elec}} = 0$ at the equilibrium position. Nevertheless, the transition can occur by nonadiabatic coupling via the kinetic energy operator. The probability for internal conversion from the vibronic state i to another vibronic manifold j is

$$P^{i\rightarrow j} = \sum_p |M^p_{\mathrm{elec}}|^2 \sum_{n_p'} \left| \left\langle \chi^j_{n_p'} \left| \frac{\partial}{\partial q_p} \right| \chi^i_{n_p} \right\rangle \right|^2 \sum_{\{n_k' \neq n_p'\}} \prod_{k \neq p} |\langle \chi^j_{n_k'} | \chi^i_{n_k} \rangle|^2 \quad (2)$$

Here, $M_{\mathrm{elec}} = \langle \psi^j | \partial / \partial q_p | \psi^i \rangle$ is the nonadiabatic interaction matrix element while p serves as the promoting vibration of the normal mode q_p. The promoting mode is the mode that couples between the electronic surfaces via its kinetic energy operator and therefore should have the correct symmetry to prevent the electronic matrix element M_{e} from vanishing. The sum over p takes into account all possible promoting modes. The last term in eq 2 is the FC factor squared for the nuclei subspace, which includes all of the nuclei coordinates except for the one that serves as the promoting mode with a summation over all of the possible divisions of the vibrational energy between the modes. In both of these cases, the FC factors strongly influence the transition probability and practically control the distribution of the electronic energy that is released in the relaxation process between the competing vibrational modes. It is useful to define the nuclear integral, $\Sigma_{\mathrm{I}\rightarrow\mathrm{F}}$, as

$$\Sigma_{\mathrm{I}\rightarrow\mathrm{F}} = \sum_{\{n'_k\}} \prod_k |\langle \chi^j_{n_k'} | \chi^i_{n_k} \rangle|^2 \quad (3)$$

for allowed transitions and as

$$\Sigma_{\mathrm{I}\rightarrow\mathrm{F}} = \sum_{n_p'} \left| \left\langle \chi^j_{n_p'} \left| \frac{\partial}{\partial q_p} \right| \chi^i_{n_p} \right\rangle \right|^2 \sum_{\{n_k' \neq n_p'\}} \prod_{k \neq \mathrm{p}} |\langle \chi^j_{n_k'} | \chi^i_{n_k} \rangle|^2 \quad (4)$$

for internal conversion via the promoting mode p. Equations 3 and 4 were explicitly written for separable states. Generalization to nonseparable states is straightforward as applied below. In both of these cases, the nuclear integral $\Sigma_{\mathrm{I}\rightarrow\mathrm{F}}$ includes the Franck−Condon factor, the nuclear part of the transition matrix element if it exists, and the final density of nuclear states.

The rate of the transition is given by the Fermi golden rule:

$$\Gamma = \frac{2\pi\kappa^2}{\hbar} \Sigma_{\mathrm{I}\rightarrow\mathrm{F}} \quad (5)$$

where κ^2 is the electronic part of either eq 1 or eq 2 for allowed transitions or internal conversion, respectively. It is often the

custom to replace $\Sigma_{I\to F}$ by the Franck−Condon factor squared multiplied by the final density of states on the accepting electronic surface. We do not do so here because as we show below a useful approximation follows from treating the final density matrix as such. In this spirit, the rate can be written as the trace over two density matrices. The rate of an allowed transition is

$$\Gamma = \frac{2\pi\kappa^2}{\hbar}\mathrm{Tr}[\hat{\rho}_f\hat{\rho}_i] \tag{6}$$

while the rate of internal conversion is

$$\Gamma = \frac{2\pi\kappa^2}{\hbar}\mathrm{Tr}[\hat{\rho}_f\hat{\rho}_i'] \tag{7}$$

The density matrices are

$$\hat{\rho}_i = \prod_k |\chi^i_{n_k}\rangle\langle\chi^i_{n_k}| \tag{8}$$

$\hat{\rho}_i'$ is defined below, and

$$\hat{\rho}_f = \sum_{\{n_k'\}}\prod_k |\chi^j_{n_k'}\rangle\langle\chi^j_{n_k'}| = \delta(\hat{H}_F - E) \tag{9}$$

where $\hat{H}_F$ is the nuclear Hamiltonian operator of the final electronic surface.

The common way to determine which vibrations are most likely to be excited is to calculate the different FC factors and the densities of final states for all possible combinations of different divisions of the energy quanta between the modes.[12] This, however, would demand an enormous computational effort and can be regarded as impossible for large molecules especially when the energy that is transferred between the degrees of freedom is large. Efficient ways to calculate FC factors are limited to the harmonic approximation.[13] Moreover, when the potential energy surface cannot be treated as separable, the eigenstates themselves are of mixed character and many will share roughly the same FC intensity, without revealing the mechanism or geometry of the jump between surfaces. Indeed, this can happen even for separable surfaces, in that many different final state FC factors could be comparable in size, reflecting the fact that the "jump" was not along any one of the separable coordinates.

2.2. Quantum-Mechanical Treatment in Phase Space. Our approach to overcome the difficulties presented in the previous section is to consider the transition in phase space. The donor state is represented by its Wigner function, the acceptor state by a classical energy hypersurface in phase space, and the transition itself is determined by the overlap between the two.

In the Wigner representation, the total FC factors squared multiplied by the final density of states are expressed as an overlap *integral* in phase space. Our method for the derivation of propensity rules is based on recognizing the points in phase space in which the nuclear *integrand* peaks. For weak transitions, the integrand that we study tends to be exponentially small, and the dominant region in phase space where this integrand peaks may often be exponentially dominant over the rest of the integral. For convenience, we use an abridged form (q,p) for the nuclear positions and momenta for the set of normal modes $(\{q_k\},\{p_k\})$, $k = 1, ..., d$.

In the Wigner phase-space representation, Γ takes the form

$$\Gamma = \frac{2\pi\kappa^2}{\hbar}\int_{-\infty}^{\infty}dq\int_{-\infty}^{\infty}dp\ \rho_F(q,p)\ \rho_I(q,p) \tag{10}$$

for an allowed transition. Here, $\rho_I(q,p)$ and $\rho_F(q,p)$ are the Wigner functions of the initial and final states density matrices, $\hat{\rho}_I$ and $\hat{\rho}_F$, respectively, defined in the usual way:

$$\rho(q,p) \equiv \left(\frac{1}{2\pi\hbar}\right)^d\int_{-\infty}^{\infty}d\eta\ \left\langle q+\frac{\eta}{2}\middle|\hat{\rho}\middle|q-\frac{\eta}{2}\right\rangle e^{-ip\eta/\hbar} \tag{11}$$

The proof of eq 10 directly follows from eq 5 with the definitions of eqs 8 and 9 for the initial and final density matrices and eq 11 for their Wigner transform. Practically, we start with the description in which each of the *initial* vibrational wave functions for each of the vibrational modes is characterized by its quasi-distribution, that is, we assume a separable system, for the excited electronic state. Consequently, the Wigner function $\rho_I(q,p)$ is a simple product of these well-defined one-dimensional quasi-distributions:

$$\rho_I(q,p) = \prod_k \rho_I^k(q_k,p_k) \tag{12}$$

For allowed transitions, we derived eqs 10, and 12 above by replacing the trace over the product of the initial and final density matrices by a phase-space integral over their respective Wigner functions. How do we generalize the approach to forbidden transitions, such as internal conversion? The new feature is that the nuclear integral as defined above in eq 4 now contains a derivative with respect to the coordinate of the promoting mode. Nevertheless, eq 10 easily generalizes to include this case by replacing the Wigner transform of the initial-state density matrix with the Wigner transform of an effective density matrix defined for the derivative of the initial state wave function. Thus, we include the derivative or any other transition operator in a redefinition of the initial state. In addition, the rate is obtained by a sum over all of the promoting modes allowed by symmetry.

The result for internal conversion is

$$\Gamma = \sum_p \Gamma_p \tag{13}$$

$$\Gamma_p = \frac{2\pi\kappa^2}{\hbar}\int_{-\infty}^{\infty}dq\int_{-\infty}^{\infty}dp\ \rho_F(q,p)\rho_I^{(p)\prime}(q,p) \tag{14}$$

where the sum is over the promoting modes and

$$\rho_I^{(p)\prime}(q,p) \equiv \rho_I^p(q_p,p_p)\prod_{k\neq p}\rho_I^k(q_k,p_k) \tag{15}$$

$$\rho_I^p(q_p,p_p) \equiv [\hat{\rho}_I^{\prime p}]_W = \left[\left|\frac{\partial\chi^i_{n_p}}{\partial q_p}\right\rangle\left\langle\frac{\partial\chi^i_{n_p}}{\partial q_p}\right|\right]_W \tag{16}$$

and $[A]_W$ stands for the Wigner transform of A. Equations 15 and 16 follow from defining the density matrix:

$$\hat{\rho}_i' = \frac{\overrightarrow{\partial}}{\partial q_p}\prod_k |\chi^i_{n_k}\rangle\langle\chi^i_{n_k}|\frac{\overleftarrow{\partial}}{\partial q_p} \tag{17}$$

For the *final* state Wigner function, $\rho_F(q,p)$, a formal expression is obtained that substantially simplifies the calculation. For relaxation processes, the final state (usually a quasi-continuum manifold of states) is defined by energy conservation to be given by the density matrix $\delta(\hat{H}_F - E)$. We define $\Delta(q,p)$ to be the Wigner transform of this delta-function density and get

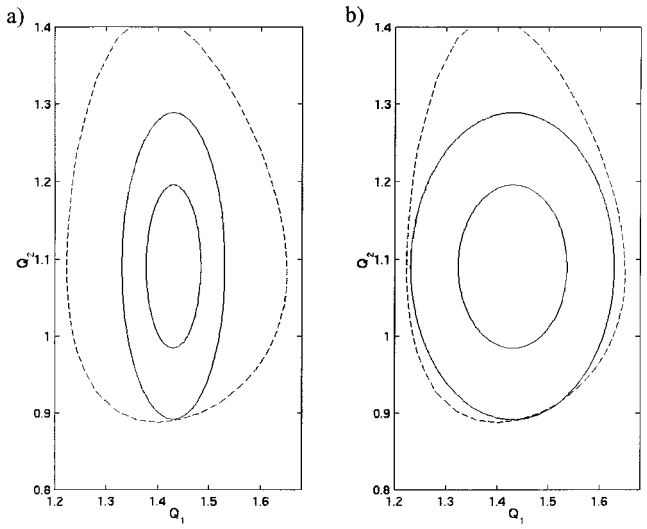

Figure 2. Geometric representation of the method for finding the direction of the quantum jump in two dimensions (Q_1,Q_2). The outer dashed ellipse represents the constraint $H_F(Q_1,Q_2) = E$. The inner solid ellipses represent the contours of the Wigner function on the upper surface. Panel a shows the case of strong maximum. The value of the Wigner function decreases rapidly with the distance from the jumping point. The jumping point is well-defined. Panel b shows weak maximum; the jumping point is not well-defined.

$$\Gamma = \frac{2\pi\kappa^2}{\hbar}\int \mathrm{d}q\ \mathrm{d}p\ \Delta(q,p)\rho_I(q,p) \tag{18}$$

for an allowed transition and

$$\Gamma_p = \frac{2\pi\kappa^2}{\hbar}\sum_p\int \mathrm{d}q\ \mathrm{d}p\ \Delta(q,p)\rho_I^{(p)\prime}(q,p) \tag{19}$$

for internal conversion. In our search for the direction of the surface jump, we look for the point(s) or region(s) in phase space (q^*,p^*) where the integrand, $\Delta(q,p)\rho_I(q,p)$ or $\Delta(q,p)$ $\rho_I^{(p)\prime}(q,p)$, peaks.

2.3. Surface Jumping. The Wigner function of the quasi-continuum final state $\Delta(q,p)$ can be expanded as an asymptotic power series in $\hbar$.[14−17] A criterion for the validity of the asymptotic series expansion is given by

$$\left(\frac{\hbar^2}{2m|\nabla V|}\right)^{1/3} < \sigma \tag{20}$$

where σ is the width of the initial wave function on the excited electronic surface, m is the reduced mass of the oscillator, and $|\nabla V|$ is the magnitude of the gradient of the surface potential at the point of the transition. The zero order of this expansion, which is in some sense a semiclassical approximation, gives

$$\Delta(q,p) \rightarrow \delta(E - H_F(q,p)) \tag{21}$$

where H_F is the classical Hamiltonian for the final (accepting) electronic state. Expansion to order $\hbar^2$ gives an Airy function instead of the delta function. An *exact* calculation of transition probabilities and rates may require more care, but the relative order of magnitudes of competing transitions as well as the partition of energy between competing accepting modes can be determined already at this semiclassical approximation level.[18]

We are looking for the phase-space point(s) (q^*,p^*) where the integrand

$$\delta(E - H_F(q,p))\rho_I(q,p) \tag{22}$$

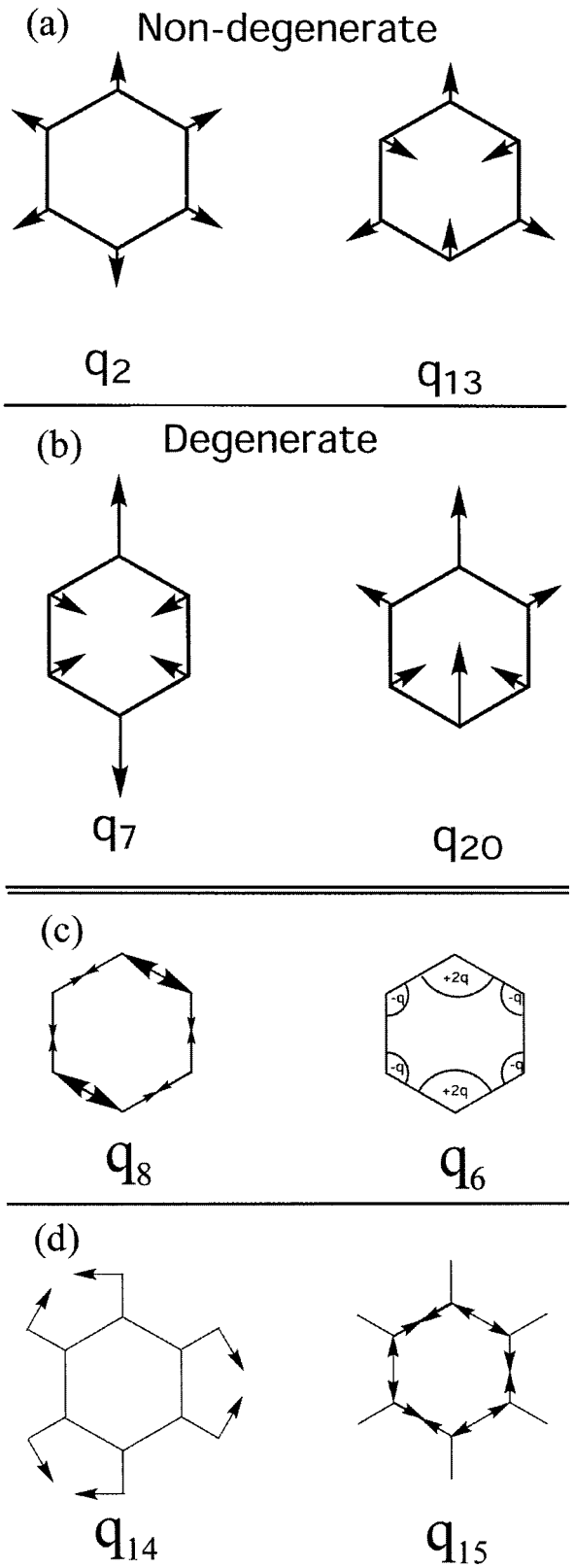

Figure 3. (a,b) The C−H in-plane stretching normal modes. Modes $q_2(a_{1g})$ and $q_{13}(b_{1u})$ are two nondegenerate modes. Mode q_2 is the totally symmetric C−H stretching. Modes $q_7(e_{2g})$ and $q_{20}(e_{1u})$ are two degenerate modes. (c) Modes q_6 and q_8, which correspond to ring deformations, are involved in a possible pseudo-Jahn−Teller effect on S_2. Both modes belong to the e_{2g} representation for the D_{6h} symmetry and to the a_g representation of the D_{2h} symmetry. (d) Modes q_{14} and q_{15} are two normal modes considered here to be involved in a possible Duschinsky rotation. Both modes belong to the b_{2u} representation; q_{14} is a ring stretching mode and q_{15} is a C−H bending mode.

is maximal, that is, we maximize the initial Wigner function $\rho_I(q,p)$ under the constraint $E = H_F(q,p)$. (For internal conversion, $\rho_I(q,p)$ is replaced by $\rho_I^{(p)\prime}(q,p)$ throughout this analysis). The location of these points in phase space gives us the phase-space jumping point(s), and from it, we deduce the accepting modes and an estimation for the energy distribution between competing modes. The value of $\rho_I(q,p)$ at these points indicates the expected strength of the transition, although we emphasize again that predictions for absolute transition rates must be based on calculation of the *integral* and the electronic prefactors; here, we are finding the dominant pathway for radiationless transition.

The geometric interpretation of the problem is demonstrated in Figure 2. The solid inner ellipses represent the contours of the Wigner function, here a Gaussian, in some two-dimensional space. The outer dashed curve is the energy surface constraint $H_F = E$. The geometric assignment is to find the points where the highest contour of the surface, $\rho_I(q,p)$, meets the constraint hypersurface, $E = H_F(q,p)$. As demonstrated in Figure 2, the strength of the extremal points can vary. Panel a shows the case in which the point of maximum of the Wigner function under the energy constraint is a *strong maximum*. In this case, there is a very rapid decrease of the Wigner function as one moves away from the extremum point on the energy constraint hypersurface. We can refer to the point as a *true* jumping point. Panel b stands as an example for a *weak* extremum. In this diagram, the Wigner function contour and the energy constraint hypersurface have a very similar curvature. A decisive jumping point is not well-defined.

2.4. Numerical Considerations. The identification of the jumping point reduces in this formalism to the mathematical problem of finding the maximum of a multidimensional nonlinear objective function under a nonlinear constraint. Simple geometric considerations show that at all of the extremum points the contours of the constant initial Wigner function are tangent to the constraint hypersurface

$$\nabla H_F = \lambda \nabla \rho_I \tag{23}$$

This condition gives a simple set of coupled algebraic equations the roots of which define the local extrema. Note that direct multidimensional local minimum finding can be converted by various computational methods (like steepest decent) to a one-dimensional search. It is considered therefore to be a much easier computational problem than a multidimensional root search of a system of nonlinear equations.[19] However, numerical methods for local minima finding under a constraint appear to have difficulties in distinguishing between local minima, maxima, and saddle points. We therefore analyze the transition in two steps. We first use a code that takes the Wigner function and the ground electronic surface potential and uses a standard routine to find extremum points (q^*,p^*) of the Wigner function under the energy constraint and the value of the Wigner function, $\rho_I(q^*,p^*)$, at these points. We then study the Wigner function on the constrained hypersurface at the vicinity of these points using algebraic considerations. The eigenvalues of a tensor of second derivatives in the subspace of the constrained phase space are calculated and the nature of each extremal point, be it a minimum, maximum, or saddle point, is determined. For some cases, especially in the harmonic approximation, the problem is also solvable analytically.[8,46]

3. Application to a 30-Dimensional Model of Internal Conversion

The model considered here is motivated by the $S_2 \rightarrow S_0$ transition in the benzene molecule.[20−28] There are theoretical and experimental indications that the benzene molecule is highly distorted on the S_2 surface and that this transition occurs via conical intersections between S_2 and S_1 and between S_1 and S_0, in particular when the initial conditions for the relaxation are a vibrationally excited state on S_2.[27−31] We consider a nonradiative transition from the vibrationless state of an S_2 electronic term to a manifold of quasi-continuum states of the $S_0(A_{1g})$ ground electronic state. In a future work, we will look at the competition between two tunneling mechanisms: that which is responsible for surface jumping considered here and that which accounts for the barrier penetration required to arrive at the conical intersection from a vibrationless initial state on the excited electronic surface. Here, we construct our model with no conical intersections. In the rest of the paper, after presenting the model, we find the jumping point for the transition, each time with a different conjecture for the potential energy surfaces (PES). In this way, we learn about the possible influences on the jump of different unknown parameters.

3.1. The Model. The following properties of benzene are imitated by our model: It has one aromatic ring of six carbons and six hydrogens. The configuration of the ground S_0 electronic state is hexagonal and belongs to the D_{6h} symmetry group. The molecule has 30 modes of vibrations, which we number according to Wilson[32] (some details are given below). The vertical energy gap between the S_0 and S_2 state is 0.228 eV.[33] The ground-state potential energy surface is taken from ref 34 (see below). The equilibrium position at S_0 is $q_1^g = 6.47$ bohr, $q_2^g = 5.02$ bohr, and $q_i = 0$ for all other normal modes by symmetry. The equilibrium position at S_2 is sometimes considered as free parameters and sometimes taken as in S_1, $q_1^g = 6.63$ bohr and $q_2^g = 5.01$ bohr.[33] Harmonic frequencies on S_2 are taken from ref 35.

Our model differs from benzene by the following properties: The potential energy surfaces that we use show no conical intersection. The transition is assumed to be a direct transition from S_2 to S_0 not going through S_1. The model assumes a planar molecule on the S_2 surface.

Normal modes that have special importance in the rest of the paper are depicted in Figure 3. Six in-plane C−H stretching modes are each an orthogonal linear combination of the six local C−H in-plane stretching modes, s_i:

$$\begin{pmatrix} q_2(a_{1g}) \\ q_7(e_{2g}) \\ q_{13}(b_{1u}) \\ q_{20}(e_{1u}) \\ q_{7a}(e_{2g}) \\ q_{20a}(e_{1u}) \end{pmatrix} = \frac{1}{\sqrt{6}} \begin{pmatrix} 1 & 1 & 1 & 1 & 1 & 1 \\ \sqrt{2} & -\frac{1}{\sqrt{2}} & -\frac{1}{\sqrt{2}} & \sqrt{2} & -\frac{1}{\sqrt{2}} & -\frac{1}{\sqrt{2}} \\ 1 & -1 & 1 & -1 & 1 & -1 \\ \sqrt{2} & \frac{1}{\sqrt{2}} & -\frac{1}{\sqrt{2}} & -\sqrt{2} & -\frac{1}{\sqrt{2}} & \frac{1}{\sqrt{2}} \\ 0 & \frac{\sqrt{6}}{2} & -\frac{\sqrt{6}}{2} & 0 & \frac{\sqrt{6}}{2} & -\frac{\sqrt{6}}{2} \\ 0 & \frac{\sqrt{6}}{2} & \frac{\sqrt{6}}{2} & 0 & -\frac{\sqrt{6}}{2} & -\frac{\sqrt{6}}{2} \end{pmatrix} \begin{pmatrix} s_1 \\ s_2 \\ s_3 \\ s_4 \\ s_5 \\ s_6 \end{pmatrix} \tag{24}$$

We take the form of the ground-state potential energy surface from ref 36 to be

$$V(\vec{q}) = \frac{1}{2}\sum_{k=1}^{30} m_k(\omega_k^g)^2(q_k - q_k^g)^2 + \frac{1}{6}\sum_{i,j,k=1}^{30} \phi_{ijk} r_i r_j r_k + O(q^4) \tag{25}$$

where

$$r_i = \sqrt{\omega_i^g m_i}(q_i - q_i^g) \tag{26}$$

Here $\omega_k^g = \tilde{\omega}_k^g[\mathrm{cm}^{-1}]/(2R_\infty)$, $q_k^g = \tilde{q}_k^g[\mathrm{cm}]/a_0$, and $m_k = \tilde{m}_k/m_e$, are the frequencies, displacements, and reduced mass of the modes of the ground electronic state, respectively, in atomic units, where R_∞, a_0, and m_e are the Rydberg constant, the Bohr radius, and the electron mass. From here on, we use the parameters in the atomic unit scale. The anharmonic force field constants, $\phi_{ijk} = \tilde{\phi}_{ijk}[\mathrm{cm}^{-1}]/(2R_\infty)$, are taken from ref 34.

3.2. A Harmonic Approximation for Both PES. Taking the initial state of S_2 to be the ground-state wave function for the normal mode k of a harmonic oscillator, we have

$$\phi_I^k(q_k) = \left(\frac{m_k\omega_k^e}{\pi\hbar}\right)^{1/4} \exp\left[-\frac{1}{2}\frac{m_k\omega_k^e}{\hbar}(q_k - q_k^e)^2\right] \tag{27}$$

where ω_k^e and q_k^e are the frequency and the equilibrium configuration of the k normal mode of the e excited electronic state, respectively. For S_2, $e = 2$. The total wave function is a product of the wave functions of each of the modes. The Wigner transform of a Gaussian wave function is another Gaussian; for mode k,

$$\rho_I^k(q_k,p_k) = \frac{1}{\pi\hbar} \exp\left[-\frac{m_k\omega_k^e}{\hbar}(q_k - q_k^e)^2 - \frac{p_k^2}{m_k\omega_k^e\hbar}\right] \tag{28}$$

The initial total Wigner function is

$$\rho_I(q,p) = \prod_{k=1}^{30}\rho_I^k(q_k,p_k) \equiv \left(\frac{1}{\pi\hbar}\right)^{30} e^{-W} \tag{29}$$

The $S_2 \rightarrow S_0$ is a forbidden transition. Therefore, when calculating the transition rates or the jumping point, the initial Wigner function, $\rho_I(q,p)$, should be replaced by $\rho_I^{(p)\prime}(q,p)$ as defined and explained in section 2.2. Taking ϕ_I^p to be as in eq 27, we get

$$\rho_I^{(p)\prime}(q,p) = \frac{m_p\omega_p^e}{\hbar}\left(\frac{m_p\omega_p^e}{\hbar}(q_p - q_p^e)^2 + \frac{p_p^2}{m_p\omega_p^e\hbar}\right)\rho_I(q,p). \tag{30}$$

The integral over the nuclear degrees of freedom giving the transition strength for internal conversion differs from the FC factor squared for an allowed transition by an additional polynomial in the integrand multiplying the Gaussian initial Wigner function. With this additional factor, the transition probability would vanish for a zero excitation of the promoting mode, and therefore, the promoting mode must have, at least, some minimal excitation.

The jumping point for an allowed transition is found by maximizing $\rho_I(q,p)$, while the jumping point for internal conversion is found by maximizing $\rho_I^{(p)\prime}(q,p)$, both under the same constraint: $H_F(q,p) = E$. It can be shown that when surface jumping occurs these two procedures give the same quantum jump. For large excitations of the promoting mode, the behavior of the Wigner function is dominated by the exponent and the influence of the polynomial is negligible. For small excitations of the promoting mode, there is, as mentioned above, a minimal amount of energy that must be transferred to the promoting mode of vibration, yet this hardly affects the quantum jump. Thus, we maximize $\rho_I(q,p)$ and not $\rho_I^{(p)\prime}(q,p)$. Therefore, we look for minima of W defined in eq 29 under the constraint $H_F(q,p) = E$.

We first consider a harmonic approximation for the Hamiltonian of the lower electronic surface:

$$H_F^h = \frac{1}{2}\sum_{k=1}^{30}\left[\frac{p_k^2}{m_k} + m_k(\omega_k^g)^2(q_k - q_k^g)^2\right] \tag{31}$$

Results of our calculations show that the extremum points (q^*,p^*) of W under the constraint $H_F^h = E$ form an 11-dimensional subspace within the 60-dimensional phase space of the problem. All of the points in this subspace include a small position excitation of the C−C totally symmetric mode (around 2% of the total energy) and an arbitrary position or momentum excitation of the six C−H in-plane stretching modes. The Wigner function $\rho_I(q,p)$ is highly peaked on this subspace with all of the points having the same value of the (argument of the) Wigner function, which is our measure of the level of propensity for a transition at these points, $W \cong 32$. Second, inspection of the C−H normal modes with the same high propensity show that they have almost the same value of $m_i\omega_i^2$ and could be considered as degenerate oscillators. We conclude the following: Within a harmonic approximation, the surface jumping is restricted to an 11-dimensional hypersurface within the 60-dimensional phase space of the problem. The surface, with $W \cong 32$, represents all of the combinations of in-plane C−H stretching modes subject to the demand of energy conservation.

3.3. Harmonic Excited PES and Anharmonic Ground Electronic Potential. In this subsection, we repeat the analysis of the previous subsection with the same initial harmonic state on the excited electronic surface but this time with the most recent anharmonic force field for the ground-state potential surface:

$$H_F = \frac{1}{2}\sum_{k=1}^{30}\left[\frac{p_k^2}{m_k} + m_k(\omega_k^g)^2(q_k - q_k^g)^2\right] + \frac{1}{6}\sum_{ijk}\phi_{ijk} r_i r_j r_k \tag{32}$$

Although adding the anharmonic force field in this asymmetric fashion does not seem self-consistent, we do so first, and then, in a following subsection, we check the possible effects of anharmonicities of the excited surface.

In Table 1, we show the points found by the numerical minimization of W under the constraint $H_F = E$. The points that have the lowest value of W, highest propensity, have an almost 6-fold degeneracy with $W \cong 17$. These points correspond to the same small position excitation of the totally symmetric C−C stretching mode and different specific combinations of the six C−H stretching modes position excitations.

TABLE 1: Local Maximum or Jumping Points Obtained for the $S_2 \rightarrow S_0$ Transition Using the Potentials of Section 3.3[a]

q_1	q_2	q_7	q_{13}	q_{20}	q_{7a}	q_{20a}	W
0.08	−0.31	−0.44	−0.31	−0.44	0	0	17.00
0.08	−0.31	−0.44	0.31	0.44	0	0	17.00
0.08	−0.32	0.22	0.31	−0.22	−0.38	−0.38	17.02
0.08	−0.32	0.22	−0.31	0.22	−0.38	0.38	17.02
0.08	−0.32	0.22	−0.31	0.22	0.38	−0.38	17.02
0.08	−0.32	0.22	0.31	−0.22	0.38	0.38	17.02

[a] The points are given in the normal-mode representation.

TABLE 2: The Points of Table 1 in the Local-Mode Representation

s_1	s_2	s_3	s_4	s_5	s_6	W
−0.76	0	0	0	0	0	17.00
0	0	0	−0.76	0	0	17.00
0	−0.76	0	0	0	0	17.02
0	0	−0.76	0	0	0	17.02
0	0	0	0	−0.76	0	17.02
0	0	0	0	0	−0.76	17.02

The data in the literature led us to perform the analysis in the normal modes of vibrations framework, yet to decode the meaning of the points, we have transformed the coordinates from normal modes to local modes using the inverse matrix of the transformation, eq 24. In Table 2, we present the same points as in Table 1 in local-mode coordinates. The physical meaning of the points is now obvious. The six points with the highest propensity refer to six equal points of local-mode excitation of C−H stretching with an addition of a very small excitation of the totally symmetric C−C stretching mode, which is the only significantly displaced mode within the 30 modes of the benzene.

3.4. Local vs Normal Coordinates. The best choice of coordinates for the description of molecular spectroscopy depends on the exact process that has to be described. Low-energy vibrational excitations such as IR absorption spectroscopy are usually described in terms of normal-mode oscillators, while high-energy processes such as dissociation are best described within a local-mode framework. It is clear that dissociation of a molecule occurs by breaking one local mode between two atoms; this is inconveniently described by high excitation of several bonds between atoms in the normal-mode description.

In our analysis, the excitation of a local C−H mode seems to have its origin in the structure of the surface potential. When the local coordinates are used, the surface potential for the six in-plane C−H stretching modes has the form

$$V = \sum_{i,j} V_{ij} s_i s_j + \sum_{i,j,k} V_{ijk} s_i s_j s_k \qquad (33)$$

Because of the symmetry of the problem $V_{11} = V_{22} = V_{ii}$, $V_{12} = V_{23} = V_{34} = V_{i,i+1}$, etc. The use of this form reduces the number of parameters that determine the third-order anharmonic surface potential to only 12 parameters (instead of 56 in the general normal description). This fact may encourage the attempt to represent the surface potential that we took from ref 34 in local modes. After this transformation of the coordinates, we have found that all of the cross coefficients in the local-mode formulation are very close to zero. We thus find that the potential represents six *separable* anharmonic oscillators. This reduces the number of parameters that describe the anharmonic potential to only *two*. The separability of the potential leads to a straightforward understanding of the reason for a local excitation found in our calculations. It can be proven that in this case of separate potentials with cubic anharmonicity the point with highest propensity corresponds to a single local excitation. We must note here also that the possibility of diagonalizing the potential in local modes was suggested already 30 years ago to understand the overtones of the C−H in-plane stretching in the IR spectrum of the benzene.[37,38] A recent treatment of empirical force constants in benzene using local modes for CH stretching was given in ref 39. Here, we started with normal modes but are forced by the results of our calculation to change to local modes.

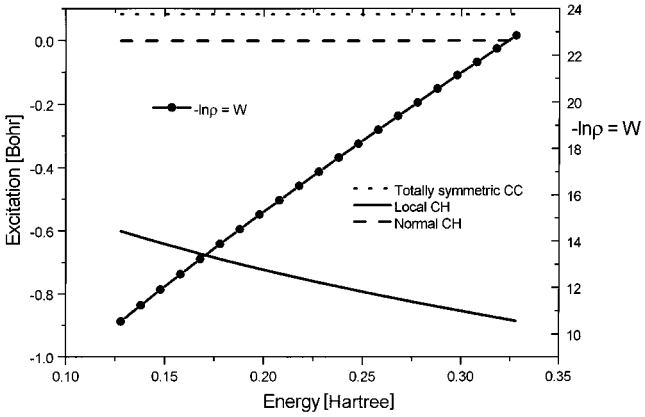

Figure 4. Results of the calculation for the $S_2 \rightarrow S_0$ transition taking the potentials of section 3.3 with the energy gap between the electronic surfaces considered as a free parameter. The coordinate and the value of the Wigner function at the jumping point are plotted vs the energy gap between the surfaces. The value of the Wigner function at the jumping point exponentially depends on the energy gap.

We summarize our conclusions so far as follows: Inclusion of anharmonic effects for the ground electronic state reduces the dimensionality of the transition from an 11-dimensional hyperspace to small regions surrounding six degenerate points. The points with the highest propensity describe a single excitation of a local mode of C−H stretching and another considerably smaller simultaneous excitation of the totally symmetric C−C stretching mode.

3.5. Sensitivity to the Energy Gap between the Two Surfaces. How sensitive are the results to the energy gap between the two potential energy surfaces? What would have changed if the energy gap was smaller or bigger? To answer that, we have taken several different hypothetical values for the energy gap and repeated the calculation for each such value, while keeping all other parameters, such as the displacements between the modes, fixed. The results are depicted in Figure 4, which shows the magnitude of the jump in different directions and the value of the Wigner function at the jumping point as a function of the energy gap between the states. We have found that most of the accepting modes undergo a vertical or an almost vertical transition, which is insensitive to the available energy. There is only one mode, here local C−H stretching, of which the excitation depends on the energy gap. This mode is excited by all of the available energy, given by the energy gap minus the energy that is required for a vertical transition of the other modes. The transition probability, estimated by the value of ρ (e^{-W}) at the jumping point, decreases exponentially with an increase of the energy gap between the surfaces. This feature is ascribed to the fact the enlargement of the gap between the surfaces leads to a larger quantum jump between them.

3.6. Influence of the Displacements between the Two Surfaces. The benzene molecule is hexagonal in the ground electronic state and, therefore, belongs to the D_{6h} symmetry group. The only modes that can have nonzero displacements under this symmetry are the totally symmetric breathing modes, that is, q_1 and q_2. If, however, the molecule is distorted on the upper surface, S_2, more modes become totally symmetric and can in principle be displaced. The possibility of an extreme change also in the frequency of these modes is not considered here.[40] How do the displacements, both for a symmetric and for a distorted upper surface, influence the jumping point?

We first take the potentials from section 3.3, implement our maximization procedure, and search for jumping points for different displacements of q_1(C−C) and q_2(C−H). Figure 5

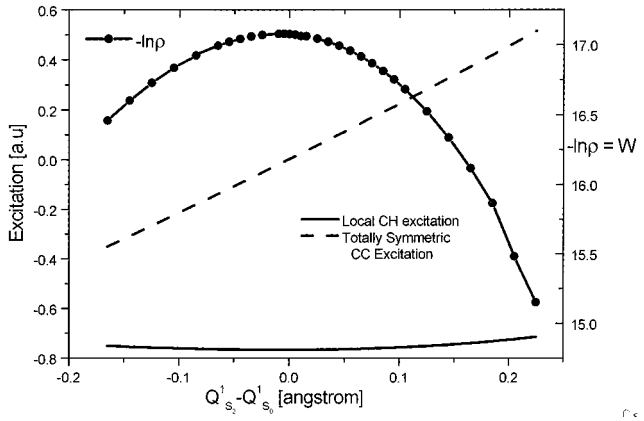

Figure 5. Results of the calculation for the $S_2 \rightarrow S_0$ transition taking the potentials of section 3.3 with the displacement of the C−C totally symmetric mode considered as a free parameter. The coordinates and the value of the Wigner function at the jumping point are plotted vs the C−C displacement between the two surfaces. The excitations of the local C−H and totally symmetric C−C stretching and the value of the Wigner function, $-\ln \rho = W$, at the jumping point are displayed in solid, dashed, and closed-circles lines, respectively. The excitation of the displaced mode linearly depends on its displacement.

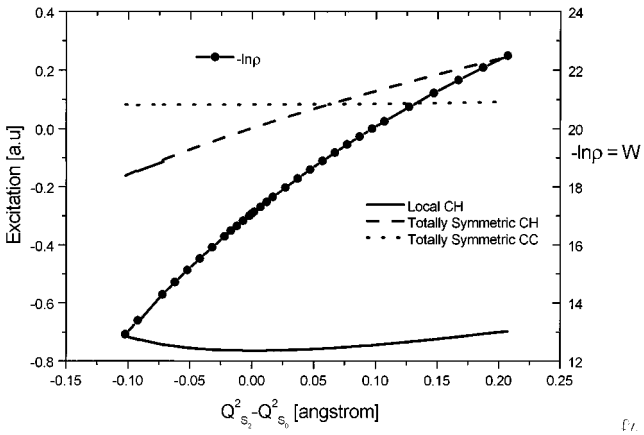

Figure 6. Results of the calculation for the $S_2 \rightarrow S_0$ transition taking the potentials of section 3.3 with the displacement of the C−H totally symmetric mode considered as a free parameter. The coordinate and the value of the Wigner function at the jumping point are plotted vs the C−H displacement between the two surfaces.

displays the nonzero coordinates of the jumping point with the highest propensity and the value of the Wigner function at this point versus the displacement of the C−C bond length. From the graph, it is easy to see that the main change of the excitation is in the C−C totally symmetric direction. The dependence is linear with a slope of almost 1.1. Changes of the C−H local excitation and of the value of the Wigner function at the jumping point are small and nonlinear. In Figure 6, we display the coordinate of the jumping point with the highest propensity and the value of the Wigner function at this point versus the displacement of the C−H bond length. Again, the excitation of the displaced mode, here the totally symmetric C−H stretching *normal* mode, is linearly proportional to the displacement (as in a vertical transition). The totally symmetric C−C is not affected at all, while the local C−H stretching mode, which is the mode that undergoes the jump, is again slightly, nonlinearly affected. Note that in this framework the normal and local C−H stretching act like almost different directions in space.

It is very likely that a distortion of the conformation of the benzene molecule takes place in the excited state because of a pseudo-Jahn−Teller (pseudo-JT) effect. Additional modes that

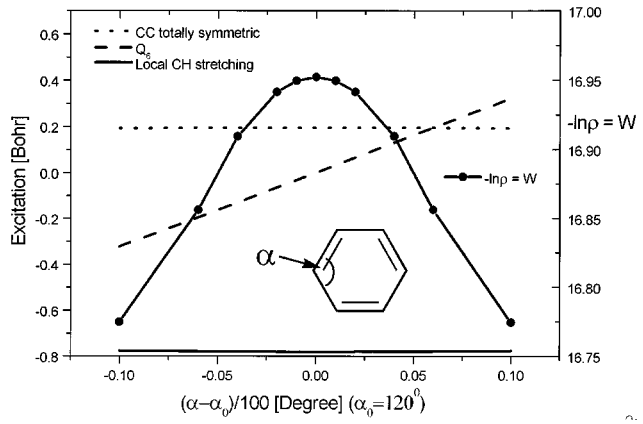

Figure 7. Results of the calculation for the $S_2 \rightarrow S_0$ transition taking the potentials of section 3.3 and including a pseudo-JT deformation of the benzene angles. The coordinate and the value of the Wigner function at the jumping point are plotted vs the difference between the angles of the benzene molecule. The excitations of the local C−H, totally symmetric C−C stretching, and q_6 modes and the value of the Wigner function, $-\ln \rho = W$, at the jumping point are displayed in solid, dotted, dashed, and closed-circles lines, respectively.

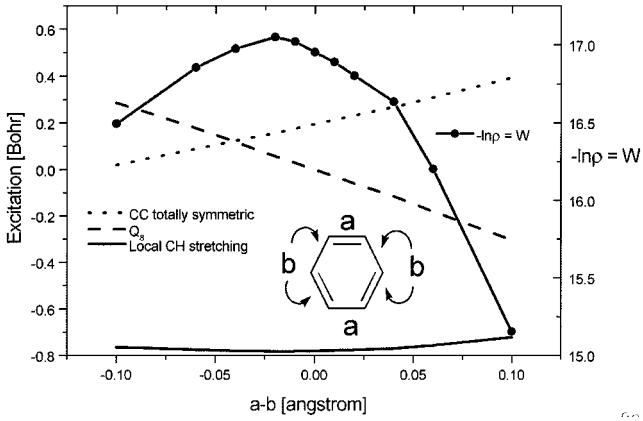

Figure 8. Results of the calculation for the $S_2 \rightarrow S_0$ transition taking the potentials of section 3.3 and including a pseudo-JT deformation of the C−C bond lengths of the benzene.

become totally symmetric under the new symmetry can have nonzero displacements. Just as an example, we consider here the case in which the molecule remains planar but belongs to the D_{2h} symmetry group. The modes that will have the most significant distortion will be the modes q_6 and q_8, which correspond to ring deformations (see Figure 3). In Figure 7, we display the nonzero coordinates of the jumping point with the highest propensity and the value of the Wigner function at this point versus the difference between the angles of the benzene ring, that is, a nonzero displacement of q_6. Again, we see that the excitation of a displaced mode, here q_6, linearly depends on the displacement. Excitations of the other modes do not significantly change. Figure 8 plots the coordinates of the jumping point with the highest propensity and the value of the Wigner function at this point versus the difference between the C−C bond lengths. This change of the bond lengths induces displacements in q_8 and q_1 and as a result a change in the coordinates of the jumping point. Even for a moderate change in the symmetry, a noticeable amount of the energy is transferred to the new modes that are displaced.

When one direction in phase space dominates the quantum jump, excitations in other directions are proportional to the displacement, as if in a vertical transition. A change of symmetry can strongly influence the jumping point.

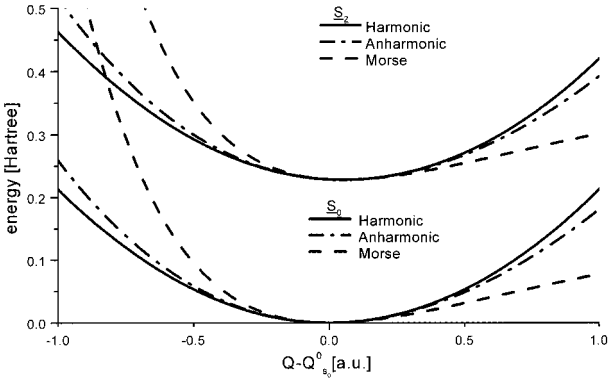

Figure 9. Local C−H stretching potentials. The harmonic, anharmonic, and Morse potentials for the local C−H stretching of the S_0 and S_2 electronic states are shown in solid, dotted-dashed, and dashed lines, respectively. The anharmonicity of the upper surface is plotted here as if equal for the two electronic states but is considered as a free parameter in the calculations.

3.7. Two Anharmonic PES. Having shown in the previous sections the separability in the subspace of C−H stretching modes of the ground surface potential, we study in this subsection the influence of the anharmonicity of the upper surface on the jumping point within the effective one-dimensional problem of a local C−H mode. Figure 9 displays the one-dimensional ground and excited electronic surface potentials in the local-mode representation. Relative to the symmetric harmonic potential, the anharmonic potential is softened on its dissociation part and has a sharper slope on its close-approach part. Applying a harmonic approximation for both surfaces gives the value of the Wigner function at the jumping point of $W \cong 32$. Taking the ground surface potential to be anharmonic gives the value of $W \cong 17$. Taking into account the anharmonicities of the excited state makes both the wave function and the Wigner function wider on the dissociation side of the potential and narrower on the close-approach side. Consequently, the value of the Wigner function at the jumping point, $W(q^*,p^*)$, gets a value between the two extremes of $32 \leq W \leq 17$.

For a quantitative analysis of this property and to make the calculation with an anharmonic potential that has a closed form expression for the initial Wigner function, we use a Morse approximation for the excited potential surface:

$$V_e(q) = D[1 - e^{-\beta(q-q_0)}]^2 \tag{34}$$

where $\beta = \sqrt{2m\omega x_e/\hbar}$ and ω, m, x_e, and $D = \hbar\omega/(4x_e)$ are the harmonic oscillator frequency, the reduced mass of the mode, the anharmonicity, and the dissociation energy of the excited electronic state. The dissociation energy for the ground electronic state is $D_g = 110.9$ kcal/mol $= 0.1701$ hartree.[41] Some experimental data, like the acidity of the benzene molecule in the excited electronic state,[42] indicate a difference of less than 10% between the dissociation energy of the excited and ground states. The dashed line in Figure 9 is the Morse potential for the above values. From the graph, it is obvious that the high-order Taylor series anharmonic force field and the Morse potential approximations are very distinct approximations. We prefer therefore to use in this subsection Morse potential for both the ground and excited states.

The wave function of the Morse oscillator is a combination of the associated Laguerre polynomials, and the Wigner function is a combination of the modified spherical Bessel function of the third kind (MacDonald function).[43,44] The Wigner function

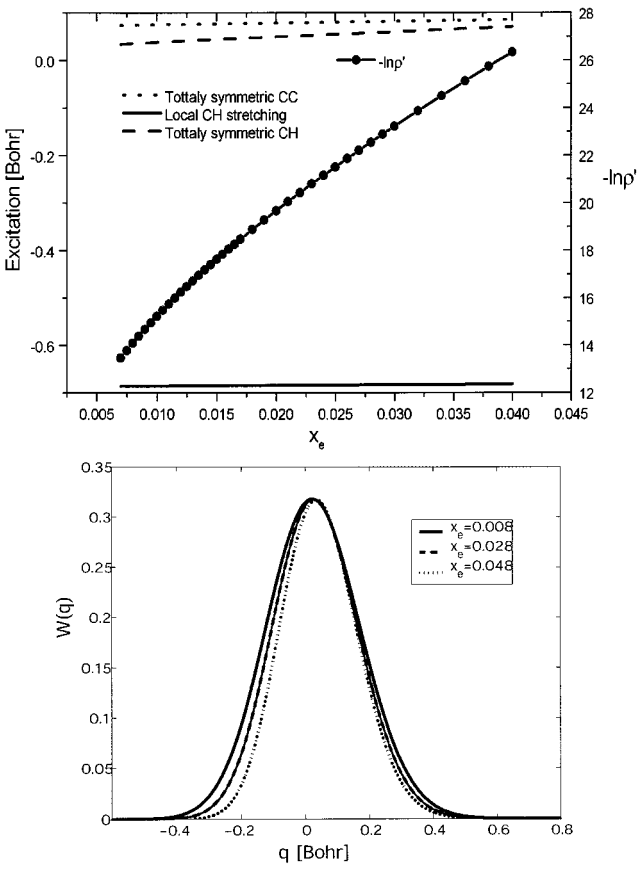

Figure 10. Panel a shows the results of the calculation for the $S_2 \rightarrow S_0$ transition taking the Morse potentials for both surfaces. The coordinate and the value of the Wigner function at the jumping point are plotted versus the anharmonicity, x_e, of the upper electronic surface. The excitations of the local C−H, totally symmetric C−C stretching, and normal C−H stretching modes and the value of the Wigner function, $-\ln \rho = W$, at the jumping point are displayed in solid, dotted, dashed, and closed-circles lines. Panel b shows the Wigner function for the Morse oscillator with $\omega = 3212\ cm^{-1}$ and different anharmonicities, x_e.

of the ground vibrational state is

$$\rho(q,p) = \frac{2}{\pi\hbar}\frac{x_e^{-2}}{\Gamma(1/x_e - 1)} e^{-2\beta(q-q_0)} K_{-2ip/(\beta\hbar)}(x_e^{-1} e^{-\beta(q-q_0)}) \tag{35}$$

where Γ is the Γ function. The order of the MacDonald function that we study is zero because the momentum at the jumping point is zero, $p^* = 0$, and we study $\rho(q,p^*)$. Figure 10b displays some examples of Wigner functions (with $p = 0$) for the same frequency, ω, but different anharmonicities, x_e. The function is a slightly deformed Gaussian in which the close-approach side of the function decays more rapidly with the increase of the anharmonicity. Figure 10a displays the projection of the jumping point with the highest propensity on the various modes and the value of the Wigner function at this point versus the anharmonicity parameter, x_e, of the upper surface, keeping the anharmonicity of the lower surface fixed. The values for W are within the qualitative predicted range discussed above. The only apparent (although small) change of the jumping point with the change of x_e is on the C−H totally symmetric normal-mode axis. The deformation of the Wigner function due to the anharmonicity x_e moves the center of the initial wave packet to the dissociation side of the potential. This change of the center of the wave packet leads to an effective positive displacement of the wave packet, and the center of the wave packet on the

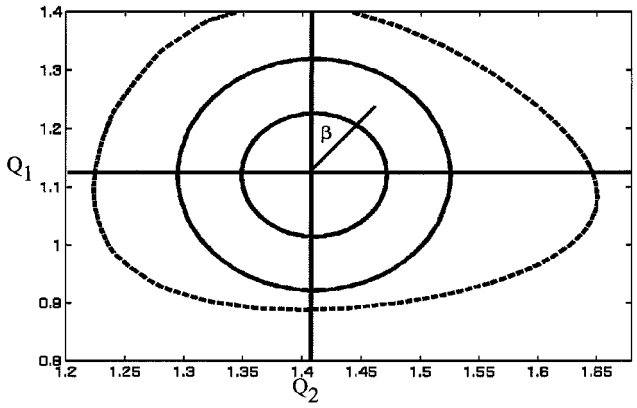

Figure 11. Geometric demonstration of the Duschinsky mode rotation in two dimensions. The solid lines represent the contours of the Wigner initial function on the excited electronic surface. The outer dashed ellipse represents the constraint surface for the lower surface $H_F = E$. Implementation of the Duschinsky rotation is done by rotating the inner ellipse by β.

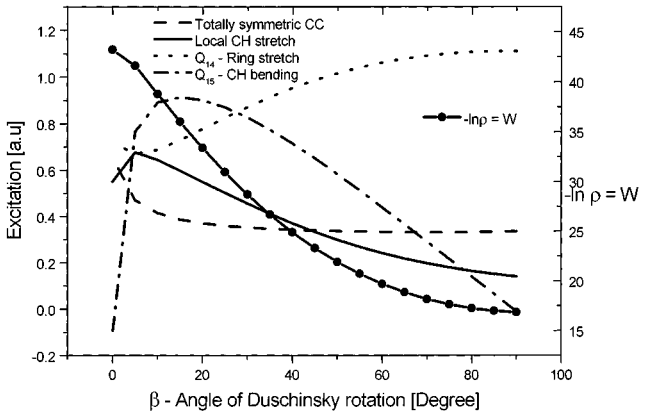

Figure 12. Results of the calculation for the $S_2 \rightarrow S_0$ transition taking the potentials of section 3.3 and including a Duschinsky mode rotation between q_{14} and q_{15}. The coordinates and the value of the Wigner function at the jumping point are plotted vs the rotation angle β. The excitations of the local C−H, totally symmetric C−C stretching, q_{14}, and q_{15} modes and the value of the Wigner function, $-\ln \rho = W$, at the jumping point are displayed in solid, dashed, dotted, dotted-dashed, and closed-circles lines, respectively.

ground electronic surface undergoes an almost vertical transition to a point in space that is displaced with respect to the ground configuration, *although there is no real displacement between the two surfaces.*

Another interesting feature that arises from the reduction of the problem to one-dimensional Morse potential regards the direction of the sudden change in the local C−H stretch. One may conclude that the wave packet lands on the ground electronic surface at the close-approach side of the potential.

An increase of the Wigner function at the jumping point is obtained with an increase of the anharmonicity of the lower surface. For a fixed anharmonicity of the lower surface, a decrease of the Wigner function at the jumping point is obtained with an increase of the anharmonicity of the upper surface. The anharmonicity on the upper surface gives correction to the two extreme approximations of harmonic−harmonic and anharmonic−harmonic potentials. Anharmonicity can induce small excitation of nondisplaced modes due to changes in the center of the initial wave packet.

3.8. Duschinsky Rotation. Consider the impact of a possible Duschinsky rotation that couples q_{14} and q_{15}. Figure 3 displays diagrams of these two modes as they appear on the ground electronic state. Suppose that the new normal modes on the excited state are mixed according to

$$\begin{pmatrix} q'_{14} \\ q'_{15} \end{pmatrix} = \begin{pmatrix} \cos\beta & \sin\beta \\ -\sin\beta & \cos\beta \end{pmatrix} \begin{pmatrix} q_{14} \\ q_{15} \end{pmatrix} \tag{36}$$

where β is the angle of rotation between the axes. According to ref 45, these two modes are coupled in this way on the first excited electronic surface. Here, we consider such a possible coupling for the second excited surface. Other conjectures for other mixing can be studied in a similar way.

The rotation in two dimensions and its influence on the jumping point is demonstrated in Figure 11. The contours of the initial Wigner function on the excited electronic surface and the constraint on the lower surface, $H_F = E$, are plotted by solid and dashed lines, respectively. The implementation of the Duschinsky rotation is done by rotating the inner ellipse by the angle β. A larger difference between the widths of the Wigner function would increase the effect of the rotation. The effect has to be considered in position as well as in momentum space. However, in our calculations, no momentum excitation is found. We first examine the case $\beta = 90°$, that is, $q'_{14} = q_{15}$ and $q'_{15} = -q_{14}$, and find a new couple of points with high propensity with a large excitation of q_{14} and small excitations of the totally symmetric C−C and C−H stretching, q_1 and q_2. The value of W at these points is 16.8, very close to the value of the points with the highest propensity found without the Duschinsky rotation. The new point that we have found for the extreme rotation is used as an initial point for a local minimum search for different angles of rotation. In Figure 12, we display this local minimum, which is found in our calculations, and the value of the Wigner function at this point versus β, the rotation angle.

A new jumping point with significant propensity develops only for angles of rotation above 65°. For smaller rotations, the point that originates from a rotation exists as a local minimum but has a very high value of W, which makes the probability of decaying through this channel negligible.

Duschinsky effect can cause, in general, a change of the direction of the quantum jump, but for the model considered here, the angles for rotation needed for this feature to appear are nonphysical.

4. Summary and Conclusions

The mechanism of surface jumping complements the mechanism of Tully−Preston's surface hopping by extending it to Franck−Condon suppressed transitions. In this paper, the surface jumping approach to nonvertical transitions was developed into a general "ready to use" tool. The formalism was first extended to include forbidden transitions, in particular, internal conversion. This results in an additional factor in the FC integrand, a polynomial of the position and momentum of the promoting mode of vibration. In most cases, the influence of the polynomial term on the direction of the jump can be neglected. More generally, the maximization procedure with this additional term is mathematically equivalent to the consideration of a decay not from the ground vibrational state but from a vibrationally excited state. This deserves further study in the future. A numerical prescription for analyzing the jump was developed for transitions between any general potential energy surfaces, including, in particular, distorted and anharmonic surfaces. The surface jumping method allows a simple determination of the accepting modes even for systems with a very large dimension.

The surface jumping method for nonvertical transitions was then applied to recognizing accepting modes in a complex model inspired by the $S_2 \rightarrow S_0$ transition in benzene. The transition takes place through nonradiative internal conversion and a large

energy of 0.228 hartree is released to the vibrational degrees of freedom of the ground S_0 state. We note that experiments have determined the decay rate of the vibrationally excited S_2 state to the S_0 electronic state to be at the scale of tens of femtoseconds. This supports the suggestion that the decay occurs via conical intersections between the S_2, S_1, and S_0 surfaces. Here, we have ignored the conical intersections and concentrated on a direct quantum jumping process. Future work should address the general question of competing tunneling mechanism, that of surface jumping and that of tunneling through a barrier to get to a conical intersection from an initial vibrationless state. The model incorporates an exact, state of the art potential surface for the ground electronic state but a simplistic treatment of the excited electronic state. Dependence on the excited-state features is tested by treating as free parameters the energy gap, displacements, and anharmonicities. We observe that for a large energy gap the masses and frequencies become the defining parameters for choosing the accepting mode, while for smaller energy gaps the displacements are more important. Anharmonicities are very important when a competition between degenerate modes occurs. These conclusions are demonstrated by the specific model considered here but apply in general to any weak internal conversion process.

For the model considered here, we found that the C−H modes undergo the jump. We showed that the jump takes place in the *local* C−H modes: Because the energy gap between the states is large compared to the vibrational energy scale and the ratio of the harmonic frequencies between the surfaces does not differ very much from 1 ($0.7 < \omega_k^e/\omega_k^g < 1.2$), the modes with the largest frequency and smallest reduced mass are the modes that undergo the jump. The *local* C−H in-plane stretching modes take almost all of the electronic energy, while all of the other modes decay almost vertically.

This finding can be interpreted also within the well-known "most probable escape path" principle of the tunnelling phenomena. Because in tunneling the competition is between channels with exponentially small probabilities, there is usually only one channel that dominates. The picture of one mode that undergoes quantum jump while the other modes decay vertically was demonstrated in several ways in the paper, for example, by altering the energy gap between the surfaces, by adding anharmonicities, and by changing the displacement of various modes.

Some of the issues to be considered in the future include transitions from thermal distributions, rotations, and an implementation of the method to other molecules. Application to dissociation, the coupling of the vibrational space of the molecule to additional degrees of freedom of a medium, the dynamics of the molecular wave packet after the quantum jump between the surfaces takes place, and the calculation of the rate using the phase-space method could also be studied within this approach.

Acknowledgment. B.S. gratefully acknowledges useful discussions with Prof. Benjamin Scharf. This research was supported by a grant from the United States−Israel Binational Science Foundation (BSF), Jerusalem, Israel, and by the National Science Foundation through a grant for the Institute for Theoretical Atomic and Molecular Physics (ITAMP) at the Harvard-Smithsonian Center for Astrophysics.

References and Notes

(1) Preston, R. K.; Tully, J. C. *J. Chem. Phys.* **1971**, *54*, 4297.

(2) Herman, M. F. *J. Chem. Phys.* **1995**, *103*, 8081; **1999**, *110*, 4141; **1999**, *111*, 10427 and references therein.

(3) Ben-Nun, M.; Quenneville, J.; Martinez, T. J. *J. Phys. Chem. A* **2000**, *104*, 5161. Hack, M. D.; Wensmann, A. M.; Truhlar, D. G.; Ben-Nun, M.; Martinez, T. J. *J. Chem. Phys.* **2001**, *115*, 1172 and references therein.

(4) Medvedev, E. S.; Osherov, V. I. *Radiationless Transitions in Polyatomic Molecules*; Springer: Berlin, 1995.

(5) Landau, L. D.; Lifshitz, E. M. *Quantum Mechanics*; Pergamon: London, 1958; Chapter 7.

(6) Medvedev, E. S. *Chem. Phys.* **1982**, *73*, 243; *J. Chem. Phys.* **1994**, *100*, 7192.

(7) Nikitin, E. E.; Noda, C.; Zare, R. N. *J. Chem. Phys.* **1993**, *98*, 46. Nikitin, E. E.; Pitaevskii, L. P. *Phys. Rev. A* **1994**, *49*, 695. Karni, Y.; Nikitin, E. E. *J. Chem. Phys.* **1994**, *100*, 2027, 8065; *Chem. Phys.* **1995**, *191*, 235.

(8) Segev, B.; Heller, E. J. *J. Chem. Phys.* **2000**, *112*, 4004.

(9) Heller, E. J.; Beck, D. *Chem. Phys. Lett.* **1993**, *202*, 350.

(10) Englman, R. *The Jahn−Teller Effect in Molecules and Crystals*; Wiley-Interscience: London, New York, 1972. Englman, R. *Non-Radiative Decay of Ions and Molecules in Solids*; North Holland Pub. Co.: Amsterdam, 1979.

(11) Jortner, J.; Rice, S. A.; Hochstrasser, R. M. *Adv. Photochem.* **1969**, *7*, 149.

(12) Osherov, V. I.; Medvedev, E. S. *Opt. Spectrosc. (Transl. of Opt. Spektrosk.)* **1990**, *67*, 53.

(13) Toniolo, A.; Persico, M. *J. Comput. Chem.* **2001**, *22*, 968 and references therein.

(14) Heller, E. J. *J. Chem. Phys.* **1978**, *68*, 2066.

(15) Heller, E. J.; Brown, R. C. *J. Chem. Phys.* **1983**, *79*, 2226.

(16) Hüpper, B.; Eckhardt, B. *Phys. Rev. A* **1998**, *57*, 1536.

(17) Hüpper, B.; Eckhardt, B. *J. Chem. Phys.* **1999**, *110*, 11749.

(18) The small parameter for the expansion is $s = [\hbar/\sqrt{2m|\nabla V|}]^{2/3}/\sigma$. In ref 17, $s \approx 0.6$ was small enough to ensure convergence. Here, the Gaussian on the excited surface has a width of $\sigma = \sqrt{\hbar/(m_k\omega_k^e)} \approx 0.2$, while the gradient of the ground potential surface at the jumping point is $|V'(q^*)| \approx 1$, $m \approx 2000$, and $s \approx 0.3$. In ref 17, higher order terms were also calculated, yet this was within a calculation for the rate. Here, we calculate propensities, which are controlled by the leading order term in the expansion.

(19) Press, W. H.; Teukolsky, S. A.; Vetterling, W. T.; Flannery, B. P. *Numerical Recipes*; Cambridge University Press: Cambridge, U.K., 1986; p 635.

(20) Shindo, K.; Lipsky, S. *J. Chem. Phys.* **1966**, *45*, 2292.

(21) Burland, D. M.; Robinson, G. W. *J. Chem. Phys.* **1969**, *51*, 4548.

(22) Burland, D. M.; Castro, G.; Robinson, G. W. *J. Chem. Phys.* **1970**, *52*, 4100.

(23) Parmenter, C. S.; Schuyler, M. W. *Chem. Phys. Lett.* **1970**, *6*, 339.

(24) Nakashima, N.; Yoshihara, K. *J. Chem. Phys.* **1983**, *79*, 2727.

(25) Sekreta, E.; Reilly, J. P. *Chem. Phys. Lett.* **1988**, *149*, 482.

(26) Buma, W. J.; van der Waals, J. H.; van Hemert, M. C. *J. Chem. Phys.* **1990**, *93*, 3733.

(27) Radloff, W.; Stert, V.; Freudenberg, T.; Hertel, I. V.; Jouvet, C.; Dedonder-Lardeux, C.; Solgadi, D. *Chem. Phys. Lett.* **1997**, *281*, 20.

(28) Tsai, S.-T.; Lin, C.-K.; Lee, Y. T.; Ni, C.-K. *J. Chem. Phys.* **2000**, *113*, 67.

(29) On conical intersections in general, see, for example: Yarkony, D. R. *J. Phys. Chem. A* **2001**, *105*, 6277 and references therein.

(30) Palmer, I. J.; Ragazos, I. N.; Bernardi, F.; Olivucci, M.; Robb, M. A. *J. Am. Chem. Soc.* **1993**, *115*, 673.

(31) Smith, B. R.; Bearpark, M. J.; Robb, M. A.; Bernardi, F.; Olivucci, M. *Chem. Phys. Lett.* **1995**, *242*, 27.

(32) Wilson, E. B., Jr.; Decius, J. C.; Cross, P. C. *Molecular Vibrations and Theory of Infrared and Raman Vibrational Spectra*; McGraw-Hill Book Company: New York, 1955; Chapter 10.

(33) Ziegler, L. D.; Hudson, B. S. *Excited States* **1982**, *5*, 41.

(34) Miani, A.; Cane, E.; Palmieri, P.; Trombetti, A.; Handy, N. C. *J. Chem. Phys.* **2000**, *112*, 248.

(35) Sension, R. J.; Brudzynsky, R. J.; Li, S.; Hudson, B. S. *J. Chem. Phys.* **1992**, *96*, 2617.

(36) Papoused, D.; Aliev, M. R. *Molecular Vibrational−Rotational Spectra*; Elsevier: Amsterdam, 1982; Chapter 23.

(37) Henry, B. R.; Siebrand, W. J. *Chem. Phys.* **1968**, *49*, 5369.

(38) See also: Halonen, L. *Chem. Phys. Lett.* **1982**, *87*, 221 and references therein.

(39) Rashev, S. *J. Phys. Chem. A* **2001**, *105*, 6499.

(40) Remarkable changes of the frequencies of q_6 and q_8 (mostly in the triplet state but maybe also in the singlet) were considered, for example, in: Scharf, B. *Chem. Phys. Lett.* **1979**, *68*, 242 and in ref 26.

(41) *Handbook of Physical and Chemistry Constants*; Clarl, S. P., Jr., Ed.; Springer: Berlin, 1990.

(42) Ireland, J. F.; Wyatt, P. A. H. *Adv. Phys. Org. Chem.* **1976**, *12*, 131.

(43) Lee, H. W. *Phys. Rep.* **1995**, *259*, 147.

(44) Frank, A.; Rivera, A. L.; Wolf, K. B. *Phys. Rev. A* **2000**, *61*, 4102.

(45) Fischer, G. *Vibronic Coupling*; Academic Press: London, 1984.

(46) Sergeev, A. V.; Segev, B. *J. Phys. A: Math. Gen.* **2002**, *35* (7), 1769−1789.